THE JOURNAL OF BIOLOGICAL CHEMISTRY
Vol. 280, No. 36, Issue of September 9, pp. 31999–32008, 2005
Printed in U.S.A.


# Ligand-assisted Aggregation of Proteins

## DIMERIZATION OF SERUM AMYLOID P COMPONENT BY BIVALENT LIGANDS*[S]

Received for publication, April 21, 2005, and in revised form, June 16, 2005
Published, JBC Papers in Press, July 20, 2005, DOI 10.1074/jbc.M504403200

**Jason G. S. Ho‡§**, Pavel I. Kitov¶§, Eugenia Paszkiewicz¶, Joanna Sadowska¶, David R. Bundle¶, and Kenneth K.-S. Ng‡‖**

*From the Alberta Ingenuity Centre for Carbohydrate Sciences at the ¶Department of Chemistry, University of Alberta, Edmonton, Alberta T6G 2G2, Canada and the ‡Department of Biological Sciences, University of Calgary, Calgary, Alberta T2N 1N4, Canada*

**A comprehensive series of solution and crystallographic studies reveal how simple, achiral, bivalent ligands of the cyclic pyruvate of glycerol promote face-to-face complex formation of the pentraxin, serum amyloid P component (SAP) into decamers. SAP, a protein of the human innate immune system, is universally present in amyloids, including cerebral amyloid deposits found in the brain of Alzheimer disease patients. Removal of SAP through a specific aggregation mechanism mediated by multivalent ligands appears to provide therapeutic benefit in the progression of this disease. Crystallographic studies reveal that in our novel series of ligands only the methyl and carboxylate moieties of the pyruvate ketal directly interact with the protein, but the geometric constraints imposed by the tether dictate which of two chair conformations are adopted by the pyruvate dioxane ring. Solution studies, as interpreted through a simple thermodynamic model, account for the distribution of pentameric and decameric bound states at different ligand concentrations and indicate that differences in the flexibility of the tether determine the geometry and stability of the specific aggregates formed between SAP and two different bivalent ligands. The factors affecting the design of ligands promoting face-to-face protein dimerization as well as potential biological implications are discussed.**

The design, synthesis, and characterization of tailored multivalent ligands is currently a rapidly expanding frontier for novel pharmaceuticals (1). In our design of inhibitors for the radially symmetric, pentameric bacterial toxins of *Escherichia coli* 0157, we observed that tailored multivalent ligands could provide a dramatic amplification in avidity over monovalent ligands (2). This design principle was subsequently validated for the structurally related cholera toxin and heat-labile enterotoxin (3, 4). Besides inhibition enhancements, aggregation of receptors is essential for triggering a variety of biological responses; *e.g.* dimerizer-regulated gene expression offers pharmacological regulation to gene therapies (5). Although the multivalency effect caused by ligand chelation can be readily rationalized in general (6, 7), the structural and design principles of the aggregation mechanism are not well understood.

Serum amyloid P component (SAP)[1] belongs to the pentraxin family of circulating serum proteins and is characterized by 5-fold radial symmetry of the identical, noncovalently associated subunits. A part of the innate immune system, SAP binds a variety of ligands, including proteins, carbohydrates, and nucleic acids, in a $Ca^{2+}$-dependent manner. SAP seems to provide marginal advantage in fighting certain infections, but its primary role is believed to be the disposal of cellular debris released by apoptotic and necrotic cells, thereby preventing autoimmunity (8–10). As a universal component of abnormal amyloid deposits, including the cerebral amyloid beta of Alzheimer disease, P component plays a role in protecting fibrils from proteolysis and promoting amyloid deposition both *in vitro* and *in vivo* (11, 12). Inhibition of SAP has recently been proposed as a pharmaceutical target, and bivalent D-proline derivatives were reported to show therapeutic efficacy in dramatically reducing serum SAP levels as well as shrinking amyloid deposits in mice (13). Despite the low intrinsic affinity of D-proline for the $Ca^{2+}$-binding site, the bivalent derivatives bridge two pentameric SAP with submicromolar activity.

To extend our current understanding of the use of multivalent ligands in the treatment of amyloid diseases, we have synthesized a series of simple but potent bivalent inhibitors of SAP that incorporate linkers of different flexibility. The interactions of two of the most potent ligands with SAP have been thoroughly characterized through solution studies including dynamic light scattering, crystal structures of SAP-ligand complexes, and a thermodynamic model for binding. These studies reveal several striking structural and thermodynamic implications of linker flexibility in multivalent binding and pose in-

* This work was supported by the Alberta Ingenuity Centre for Carbohydrate Sciences, by Canadian Institutes for Health Research Grant G118980012 (to D. R. B.), by a Canadian Institutes for Health Research New Investigator Award (to K. K.-S. N.), and by the Alberta Heritage Foundation for Medical Research. X-ray diffraction data were collected at Beamline 8.3.1 of the Advanced Light Source at Lawrence Berkeley Lab under an agreement with the Alberta Synchrotron Institute. The Advanced Light Source is operated by the Department of Energy and supported by the National Institute of Health. Beamline 8.3.1 was funded by the National Science Foundation, the University of California, and Henry Wheeler. The Alberta Synchrotron Institute synchrotron access program is supported by grants from the Alberta Science and Research Authority and Alberta Heritage Foundation for Medical Research. The costs of publication of this article were defrayed in part by the payment of page charges. This article must therefore be hereby marked "*advertisement*" in accordance with 18 U.S.C. Section 1734 solely to indicate this fact.

[S] The on-line version of this article (available at http://www.jbc.org) contains supplementary material.

*The atomic coordinates and structure factors (code 2A3W, 2A3X, and 2A3Y) have been deposited in the Protein Data Bank, Research Collaboratory for Structural Bioinformatics, Rutgers University, New Brunswick, NJ (http://www.rcsb.org/).*

§ These authors contributed equally to this work.

** Supported by a fellowship from the Alberta Ingenuity Fund.

‖ To whom correspondence should be addressed: Dept. of Biological Sciences, University of Calgary, 2500 University Dr. NW, Calgary, Alberta T2N 1N4, Canada. Tel.: 403-220-4320; Fax: 403-289-9311; E-mail: ngk@ucalgary.ca.

[1] The abbreviations used are: SAP, serum amyloid P component(s); MOβDG, methyl 4,6-(1-carboxyethylidene)-β-D-galactoside; DLS, dynamic light scattering; GFC, gel filtration chromatography; ELISA, enzyme-linked immunosorbent assay.


Supplemental Material can be found at:
http://www.jbc.org/cgi/content/full/M504403200/DC1

triguing questions regarding the factors that determine the stability of ligand-induced face-to-face protein complexes.

## EXPERIMENTAL PROCEDURES

*Gel Filtration Chromatography (GFC)*—GFC was carried out using a PerSeptive Biosystems BioCAD Sprint liquid chromatography system. For most experiments, the running buffer was TN buffer (10 mM Tris, pH 8.0, 140 mM NaCl, and 20 mM $CaCl_2$). Typically, 20 $\mu$l of protein solution (1 mg/ml SAP) in buffer A (10 mM Tris-HCl, pH 8.0, 140 mM NaCl, 1 mM EDTA) was mixed with 20 mM $CaCl_2$ and either 2′-dAMP, compound **1**, or compound **3** (each at 20 mg/ml; compounds shown in Scheme 1). The protein-ligand mixtures were equilibrated overnight at 4 °C before loading onto a Superose 6 GL 10/300 column (Amersham Biosciences) or a Zorbax GF-250 9.4/250 column (Agilent Technologies). The flow rate was 1.0 ml/min, the temperature was 25 °C, and elution was monitored by measuring absorbance at 280 nm.

*Dynamic Light Scattering (DLS)*—Hydrodynamic radius analysis was carried out at 25 °C using a Protein Solutions DynaPro molecular sizing instrument (Proterion Corp.). Samples containing SAP (0.5 mg/ml) and one of three compounds (2′-dAMP (10 mM), compound **1** (10 mM), or compound **3** (40 mM)) were equilibrated in buffer A plus 20 mM $CaCl_2$ overnight at 4 °C prior to DLS measurements. Hydrodynamic radius analysis of SAP with compounds **1** and **2** was also carried out over a range of concentrations. Samples containing SAP (1 mg/ml) and 0–10 mM of compounds **1** or **2** were equilibrated in buffer B (250 mM sodium acetate, pH 5.5, 50 mM calcium acetate) overnight at 4 °C before DLS measurements. DLS measurements were only accepted if the light intensity count rate was steady to within ±20% and the polydispersity reading was less than 20%. All of the samples were measured in triplicate.

*Crystallization*—SAP was dialyzed extensively against buffer A and concentrated to 10 mg/ml prior to crystallization. All of the crystals were grown by the hanging drop vapor diffusion method (1 $\mu$l of protein and 1 $\mu$l of ligand and 1 $\mu$l of reservoir equilibrated against 1 ml of reservoir solution) at 21 °C. Two crystal forms were grown in the presence of compound **1**. Form A (SAP·$\mathbf{1}_5$) grew at a ligand concentration of 40 mM with a reservoir solution consisting of 250 mM sodium acetate, pH 5.5, 50 mM calcium acetate, 9% (w/v) PEG 8000, 20% (w/v) PEG 400. Crystals appeared overnight and continued to grow for a week, giving approximate dimensions of 0.4 mm × 0.1 mm × 0.05 mm. Form B ($SAP_2$·$\mathbf{1}_5$) grew at a ligand concentration of 10 mM with a reservoir solution consisting of 250 mM sodium acetate, pH 5.5, 50 mM calcium acetate, 11.5% (w/v), PEG 4000, 10% (w/v) PEG 400, 5% (w/v) sorbitol. Crystals appeared after several weeks giving approximate dimensions of 0.13 mm × 0.25 mm × 0.05 mm. Crystals in the presence of compound **2** grew at a ligand concentration of 40 mM with a reservoir solution consisting of 250 mM sodium acetate, pH 5.5, 50 mM calcium acetate, 12% (w/v) PEG 8000. Crystals appeared after 3 or 4 days and continued to grow for several weeks, giving approximate dimensions of 0.4 mm × 0.05 mm × 0.03 mm. Prior to data collection, the crystals grown in the presence of compound **2** were adapted to a cryopreservation solution by transferring crystals to a 5-$\mu$l drop (250 mM sodium acetate, pH 5.5, 50 mM calcium acetate, 16% (w/v) PEG 8000, and 3% (w/v) PEG 400) and equilibrating against 1 ml of well solution (250 mM sodium acetate, pH 5.5, 50 mM calcium acetate, 16% (w/v) PEG 8000, and 30% (w/v) PEG 400) overnight.

*Structure Determination*—Diffraction data were measured from single crystals flash frozen under a nitrogen cryo stream (~110 K) using a MAR image plate and X-rays produced with a rotating copper anode (Rigaku RU300H). Higher resolution data were also measured on single crystals using an ADSC Quantum-315 CCD detector at the Advanced Light Source on Beamline 8.3.1 ($\lambda$ = 1.115 Å). The data were processed, scaled, and merged using DENZO, SCALEPACK (14), and programs from CCP4 (version 4.2.2) (15). Space group and unit cell dimensions for the three different SAP complexes are given in Table III.

The protein chains from the SAP pentamer of the 2′-dAMP complex (Protein Data Bank code 1LGN) were used as the search model for all molecular replacement calculations (16). The structure of SAP complexed with compound **1** at 40 mM (SAP·$\mathbf{1}_5$ or crystal form A) was determined using Molrep (17). A single pentamer was located in the asymmetric unit, giving rise to reasonable crystal packing and a solvent content of 57%. Refmac (version 5.1.24) (18) was initially used to carry out rigid body refinement with each of the five protomers as rigid bodies (100–2.8 Å resolution, $R_{work}$ = 0.318, $R_{free}$ = 0.308). The structure of SAP complexed with compound **1** at 10 mM ($SAP_2$·$\mathbf{1}_5$ or crystal form B) was determined using AMoRe (19). Four pentamers were located in the asymmetric unit, giving rise to reasonable crystal packing and a solvent content of 59%. AMoRe was used to carry out rigid body refinement with each protomer as a rigid body (20–3.5 Å, $R_{fac}$ = 0.331). The structure of SAP complexed with compound **2** at 40 mM concentration was determined using CNS (version 1.0) (20). Two pentamers were located in the asymmetric unit, giving rise to reasonable crystal packing and a solvent content of 52%. CNS was used to carry out rigid body refinement with each protomer as a rigid body (20–3.8 Å resolution, $R_{work}$ = 0.334, $R_{free}$ = 0.345).

Refmac was used for the refinement of individual atomic positional and temperature factor parameters, as well as translation-libration-screw axis motion parameters for each protomer. Noncrystallographic symmetry restraints were applied only for refining the structure of SAP complexed with compound **2**, because of the relatively low limit of diffraction. Xfit (21) was used for inspecting electron density maps and interactive model building. Procheck (22) and Whatcheck (23) were used to evaluate stereochemical parameters in the model. The data collection and refinement statistics for all crystal structures are summarized in Table III.

## RESULTS

*Synthesis and Activity of Novel Bivalent Inhibitors*—SAP has previously been shown to bind to a number of bacterial and plant oligosaccharides in a $Ca^{2+}$-dependent manner (24). The crystal structure of a complex of SAP and methyl 4,6-(1-carboxyethylidene)-$\beta$-D-galactoside (MO$\beta$DG) recently revealed how the cyclic pyruvate ketal moiety in many of these natural carbohydrate polymers can directly interact with the $Ca^{2+}$-binding site and adjacent regions of SAP (25). Based on this structural information, we hypothesized that a minimal fragment consisting of the cyclic pyruvate ketal of glycerol could be used to form the core binding element of a novel series of bivalent inhibitors intended to form face-to-face assemblies of SAP pentamers.

As part of a much larger series, bivalent derivatives **1** and **2** as well as monovalent analog **3** were synthesized, and the SAP binding activity for each compound was evaluated by a solid phase assay (supplementary material). These compounds have a simple, achiral structure and can be obtained in high yield from inexpensive starting materials. In this report, we focus our studies on two compounds differing primarily in the rigidity of the linker segment. The end groups and the lengths of the linkers in compounds **1** and **2** are identical, but the piperazine ring in compound **2** prevents rotation around three central bonds, thereby restricting the flexibility of the tether. As a result, the apparent binding of compound **2** to SAP, as measured by solid phase competitive ELISA, is nearly 30-fold higher than that of the more flexible analog **1**, which in turn binds 140-fold better than **3**. Balancing linker rigidity against geometric requirements for optimal orientation of the end groups is a common issue in the design of multivalent ligands. The difference in activity seen in this case prompted the additional studies described below (Scheme 1).

*Oligomeric States of SAP in Solution*—To directly observe the different oligomeric states adopted by serum amyloid P component in the presence of bivalent ligands in solution, GFC and DLS were used. As shown previously, SAP in TN buffer elutes at the same volume in the absence of any ligands and in the presence of 2′-dAMP (26) (Table I). Previously reported crystallographic and small angle x-ray scattering studies also indicate that SAP adopts two different decameric forms under these conditions (16, 27, 28). SAP in the presence of a monovalent ligand, either MO$\beta$DG or compound **3**, elutes at a larger volume, suggesting the presence of a pentameric state, which is consistent with previous crystallographic and solution studies (25, 28). SAP in the presence of compound **2** elutes at a smaller volume consistent with a decameric state, which agrees with the DLS measurements and crystallographic studies described below.

DLS confirms and provides a finer probe of oligomeric pop-

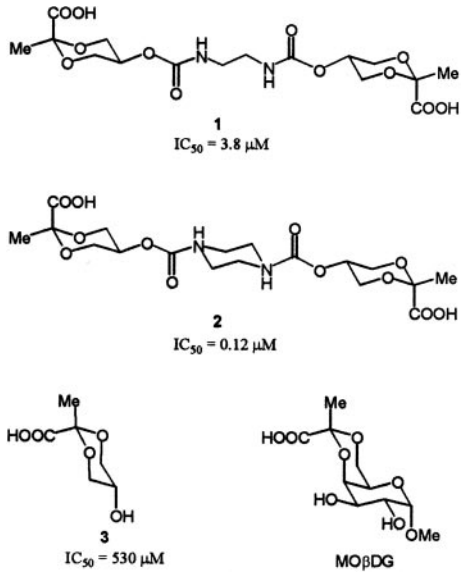


SCHEME 1. **Compounds 1–3**

TABLE I
*Gel filtration chromatography*

| | Elution volume | |
|---|---|---|
| | Superose 6 GL | Zorbax GF-250 |
| | *ml* | |
| SAP | 12.9 | 7.1 |
| SAP + **1** | 12.8 | 7.1 |
| SAP + **3** | 13.8 | 7.7 |
| SAP + 2′-dAMP | 13.0 | 7.2 |

ulations than GFC (Table II). In TN buffer, unliganded SAP and SAP bound to an excess of either 2′-dAMP or compound **2** have hydrodynamic radii ($R_h$) greater than 6 nm. In comparison, SAP bound to compound **3** in TN buffer or SAP alone in acetate buffer have hydrodynamic radii of 5.4 and 5.8 nm, respectively. The larger hydrodynamic radii in the first three samples is consistent with the presence of a decameric form as shown previously by GFC, solution x-ray scattering, and x-ray crystallography (16, 26).

DLS was also used to monitor the variation in hydrodynamic radii for samples of SAP equilibrated with varying concentrations of the bivalent compounds **1** and **2** (Fig. 1). As the concentrations of the bivalent compounds increase from 0.25 to 10 mM, the average hydrodynamic radius of the particles in solution increases from a value expected for a pentamer (designated SAP·$\mathbf{1}_5$ or SAP·$\mathbf{2}_5$) and reaches a plateau near a value expected for a decamer (designated $SAP_2$·$\mathbf{1}_5$ or $SAP_2$·$\mathbf{2}_5$). As the concentration of compound **1** is further increased, the hydrodynamic radius decreases back to the value expected for a pentamer, SAP·$\mathbf{1}_5$. In contrast, even at the highest concentrations of compound **2** that could be tested (100 mM), the hydrodynamic radius remains at the value expected for a decamer, $SAP_2$·$\mathbf{2}_5$.

To quantitatively account for the variation in populations of pentamers and decamers in solution as a function of ligand concentration, a thermodynamic model based on the principles of mass action was developed (for a complete derivation, please refer to the supplementary material). The model leads to the relationships below that permit the two variables, free receptor concentration and free ligand concentration [L], to be solved numerically at any given values of the total concentrations of ligand $[L]_o$ and receptor $[R]_o$, where $K_{pentamer}(i)$ and $K_{decamer}(i)$ are the stability constants for the formation of pentameric and decameric complexes.

$$[R]_o = [R](1 + \Sigma K_{pentamer}(i)[L]^i + 2\Sigma K_{decamer}(i)[L]^i[R]) \quad \text{(Eq. 1)}$$

TABLE II
*Dynamic light scattering*

| | Hydrodynamic radius |
|---|---|
| | *nm* |
| SAP | 6.1 ± 0.21 |
| SAP + **1** | 6.2 ± 0.30 |
| SAP + **3** | 5.8 |
| SAP + 2′-dAMP | 6.1 ± 0.06 |
| SAP in acetate | 5.4 ± 0.15 |

$$[L]_0 = [L] + \Sigma i\, K_{pentamer}(i)[L]^i[R] + \Sigma i\, K_{decamer}(i)[L]^i[R]^2 \quad \text{(Eq. 2)}$$

Stability constants for various pentameric and decameric complexes in which the receptor exists are defined as follows,

$$K_{pentamer}(i) = \frac{[RL_i]}{[R][L]^i} \quad \text{(Eq. 3)}$$

$$K_{decamer}(i) = \frac{[RL_iR]}{[R]^2[L]^i} \quad \text{(Eq. 4)}$$

where $i$ is the number of ligands in a complex; $i$ varies from 1 to 5.

Parametrization of the model relies on two intrinsic binding constants, $k$ and $K$. The "intrinsic" binding constant $k$ quantifies the strength of the interaction between each individual binding site of the receptor and a single affinity element of the ligand. A second "multivalent" binding constant $K$ quantifies the strength of the hypothetical complex, where each binding fragment of bivalent ligand engaged in interaction with single binding site of two receptor molecules. For simplicity, $K$ assumed to be constant independent of occupancy in each particular complex. The values for $k$ and $K$ may vary for different bivalent ligands and can be derived by fitting binding data to the model. The values of $k$ and $K$ can also be derived from competitive ELISA measurements under conditions at neutral pH where the binding is stronger. Accounting for the reduced binding affinity seen under the lower pH conditions used for the DLS experiments, it appears that the values of $k$ and $K$ derived from ELISA measurements are consistent with those obtained by fitting our model to the DLS data (Fig. 1). Fig. 2 shows relationships between $k$ and $K$ and corresponding stability constants $K_{pentamer}(i)$ and $K_{decamer}(i)$. The thermodynamic model and the crystallographic structures described below both help to provide a framework for understanding the basis of the differences in the binding behaviors of compounds **1** and **2**.

*Crystal Structures of SAP-Ligand Complexes*—To establish the molecular structural basis of ligand-induced SAP oligomerization, crystal structures were determined for complexes formed between SAP and compound **1** at 10 mM (decamer $SAP_2$·$\mathbf{1}_5$) and at 40 mM (pentamer SAP·$\mathbf{1}_5$) (crystal forms A and B, respectively), as well as for SAP bound to compound **2** at 40 mM (Table III). The oligomeric forms seen in the crystal structures are consistent with the distributions of oligomeric forms observed by DLS at different concentrations of compounds **1** and **2**. Most surprisingly, however, compound **2** forms a decamer in which two of the expected ligands for the complex $SAP_2$·$\mathbf{2}_5$ are absent, producing a complex $SAP_2$·$\mathbf{2}_3$ with only three bivalent ligands present.

In all of the complexes, the carboxylate group of the cyclic pyruvate ketal ring in each ligand coordinates directly to the two calcium ions of a single SAP protomer (Fig. 3). Direct interactions between negatively charged groups and both calcium ions are a common feature of the three previously characterized SAP complexes with 2′-deoxy-AMP (16), MOβDG (25), and a bivalent D-proline analog (13). Each carboxylate

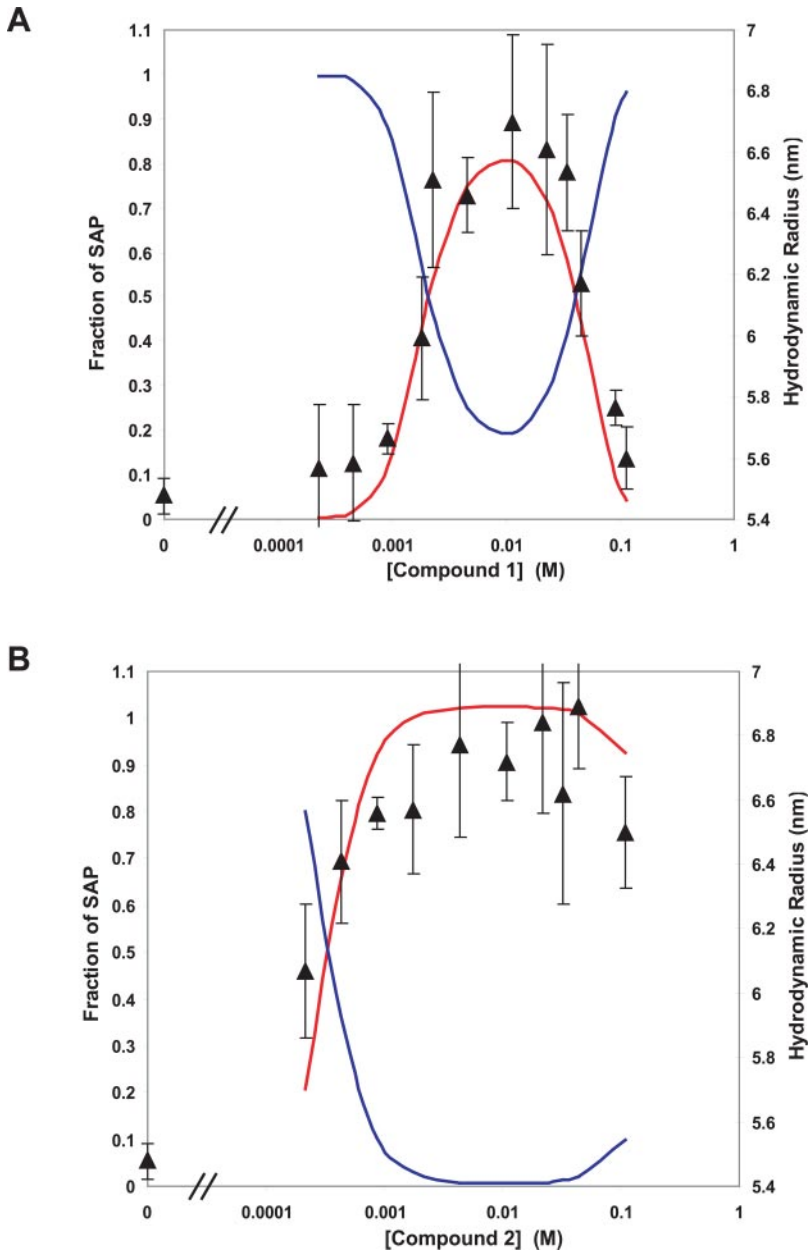


FIG. 1. **DLS measurements (derived hydrodynamic radius) are superimposed onto distribution curves showing the fractions of pentameric (*blue line*) and decameric (*red line*) forms of SAP that are predicted from the theoretical mass action model for compounds 1 (*A*) and 2 (*B*).** The values of the model parameters are $k = 50$, $K = 2400$ (*A*); $k = 50$, $K = 10{,}500$ (B). The model assumes a maximal ligand occupancy of 5 for the formation of sandwich-like complexes consisting of two face-to-face pentamers.

oxygen atom directly coordinates to one calcium ion while simultaneously accepting a bifurcated hydrogen bond donated from a calcium ligand ($Asn^{59}$ and $Gln^{148}$) and shared with an oxygen acceptor within the pyruvate ketal ring (Fig. 3). The only other direct interactions between the protein and the ligand consist of van der Waals' contacts between the ligand methyl group and a hydrophobic pocket formed by side chains from $Leu^{62}$, $Tyr^{64}$, and $Tyr^{74}$. This hydrophobic contact is also seen in the complex between SAP and MO$\beta$DG (25).

In the decameric complexes $SAP_2{\cdot}\mathbf{1}_5$ and $SAP_2{\cdot}\mathbf{2}_3$, separate pentamers are cross-linked by multiple bivalent ligands (Figs. 4 and 5). In the decameric complex $SAP_2{\cdot}\mathbf{1}_5$, the planes of the two pentamer rings are nearly parallel (interplanar angle of 0.8°). All 10 $Ca^{2+}$-binding sites are occupied by ligand in the same conformation, and the $Ca^{2+}$-$Ca^{2+}$ distances for each pair of cross-linked protomers lies within the range of 17.2–19.4 Å. A similar situation is seen in the decameric complex formed with 2′-deoxy-AMP (16) (interplanar angle of 0.1°, $Ca^{2+}$-$Ca^{2+}$ distances in the range of 10.9–11.0 Å). In contrast, the decameric complex $SAP_2{\cdot}\mathbf{2}_3$ shows that the two pentamer rings are tilted relative to each other (interplanar angle of 4.6°). Moreover, only six of the 10 $Ca^{2+}$-binding sites are occupied by ligand, with three pairs of opposing protomers being cross-linked by bivalent ligands and the remaining four protomers free of bound ligand. The $Ca^{2+}$-$Ca^{2+}$ distances range from 14.7 to 16.2 Å in the three pairs of protomers cross-linked by bivalent ligands and are 12.0 and 12.2 Å for the two pairs of unliganded protomers.

## DISCUSSION

Multivalent ligand-induced aggregation provides an attractive approach to the development of novel therapeutics in a wide range of medically important areas. Many viral, bacterial, and fungal pathogens adhere to cell surface protein and carbohydrate epitopes through multivalent ligand-receptor interactions, and synthetic inhibitors mimicking the multivalent nature of these interactions have been shown to provide effective therapeutics in a number of systems. The presentation of five binding sites on a single face of the SAP pentamer and the unique role of SAP in promoting amyloid plaque formation in diseases such as Alzheimer disease and type II diabetes provide an opportunity for the development of novel multivalent

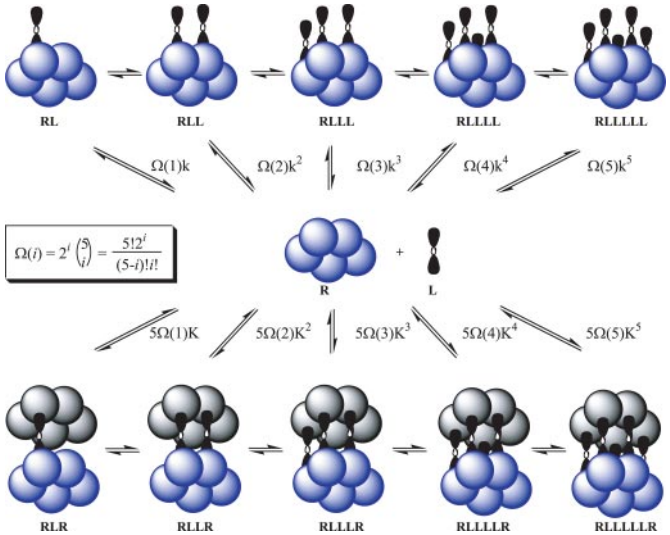


FIG. 2. **Schematic diagram showing free energy relationships between the unbound receptor and complexes with ligand.** Expressions next to equilibrium signs represent corresponding equilibrium constants $K_{\text{pentamer}}(i)$ and $K_{\text{decamer}}(i)$.

ligands that promote the disruption of amyloid plaques. The principles underlying the design and mechanism of multivalent ligands for therapeutic purposes remain poorly understood, however, and studies into the basic interactions between multivalent ligands and SAP are needed to develop more effective therapeutics.

The binding of multivalent ligands to oligomers bearing multiple binding sites gives rise to a complex equilibrium of oligomeric states that depends on both the single-site and multi-site binding affinities of different multivalent ligands. To quantitatively model binding states in this complex system, we have developed a simple, thermodynamic model that predicts the distribution of different bound forms of receptor in solution (corresponding to observations from ELISA, DLS, and GFC) as a function of bivalent ligand concentration (Fig. 2).

The difference in stability of the complexes formed by compounds **1** and **2** is consistent with the higher inhibitory potency of compound **2** in the solid phase ELISA and with entropy penalties associated with the increased flexibility of compound **1**. Compound **1** is free to rotate about the three single bonds of the tether, and in principle each bond may adopt each of three staggered rotamers. Therefore $K_{\text{decamer}}$ (the quantity estimated by ELISA) is expected to be reduced by a factor of $\sim 3^3$. The "bell" shape of the binding isotherms seen in DLS cannot be observed by ELISA, because the aggregated decameric species are replaced with pentameric complexes whose binding sites are highly populated with monovalently bound ligand at high ligand concentrations. These species are also inhibited and unable to bind to the plate. The model predicts that under the conditions used for ELISA, the observed inhibition isotherm coincides with the left branch of the bell formed by combined aggregated species (decamers), and $K$ can be closely approximated by $1/IC_{50}$.

In acetate buffer, GFC and DLS both indicate that unliganded SAP adopts a predominantly pentameric state. As the concentrations of bivalent ligands increase, DLS indicates that the average hydrodynamic radius of protein complexes in solution increases, which in turn suggests a decrease in the proportion of pentamers and an increase in the proportion of decamers (Fig. 1). For compound **1**, the average hydrodynamic radius of particles in solution reaches a maximum value that is similar to that expected for a pure population of decamers over the concentration range of ~5–20 mM. At higher concentrations, the hydrodynamic radius appears to decrease, suggesting a decrease in the proportion of decamers and an increase in the proportion of pentamers. For compound **2**, the hydrodynamic radius reaches a similar maximum value over the concentration range of ~1–100 mM, but higher concentrations could not be tested because of the limited solubility of the compound.

The variation in hydrodynamic radius observed by DLS provides quantitative support for the distribution of oligomeric states predicted by the mass action model (Fig. 1). The values of $k$ and $K$ used to fit the DLS data (Fig. 1) are comparable with values that were estimated by competitive ELISA measurements (supplementary material). It is notable that ELISA measurements indicate weaker binding of both compounds **1** and **2** at the lower pH conditions (5.5) used for DLS measurements and crystallization, when compared with binding measurements conducted at physiological pH 7–8. The decameric complex seen in crystals formed in the presence of compound **1** at 10 mM, the pentameric complex seen in crystals formed with compound **1** at 40 mM, and the decameric complex seen in crystals formed with compound **2** at 40 mM are also consistent with the DLS data and support the binding model.

Despite similar local interactions between the carboxylate and methyl groups of the ligand with the protein and compounds **1** or **2**, it is striking that the dioxane ring adopts different conformations in different complexes (Fig. 4). In the SAP·$\mathbf{1}_5$ complex, the ring adopts a chair conformation in which the carboxylate group is axial, whereas the methyl group and linker oxygen are equatorial. This appears to be the major conformation adopted by the ring, but residual difference electron density indicates that a mixture of ring conformations may be present. In contrast, in both bivalent complexes $SAP_2$·$\mathbf{1}_5$ and $SAP_2$·$\mathbf{2}_3$, an alternate chair conformation is clearly adopted in which the carboxylate group is equatorial, whereas the methyl group and linker oxygen are axial. Although the opposite conformation with the axial carboxylate group is the only one observed by NMR for the free ligand in solution, specific geometric constraints for orienting face-to-face pentamers in a decameric complex act to select the alternate chair conformation of the dioxane ring. The induced fit conformations of the bound ligands indicate that the gain in binding energy caused by multivalency is partially offset by the energetic penalty associated with the adoption of an alternate conformation of the pyruvate ketal ring. This unexpected observation indicates that any rational design of ligands would have to consider both conformations of the dioxane ring.

The structures of the decameric complexes $SAP_2$·$\mathbf{1}_5$ and $SAP_2$·$\mathbf{2}_3$ provide a starting point for understanding the geometric requirements for the formation of complexes between two SAP pentamers and multiple bivalent ligands. For the complex SAP·$\mathbf{1}_5$ cross-linking is not observed between different pentamers. A single ligand is bound to each calcium-binding site, with well defined electron density around the dioxane ring but no electron density corresponding to the linker or second ring, which are presumably mobile and disordered in the crystals.

A detailed structural analysis of the complexes $SAP_2$·$\mathbf{1}_5$ and $SAP_2$·$\mathbf{2}_3$ suggests that the different linker structures of these two bivalent ligands may contribute to the different arrangements of pentamers within the two decameric complexes. The more flexible linker found in compound **1** appears to accommodate a parallel arrangement of pentamers that allows all 10 binding sites to be occupied by ligand in a highly symmetrical arrangement. In contrast, the more rigid linker found in compound **2** imposes a stronger conformational constraint on the arrangement of opposing pentamers. The geometric requirements of the linkers induces a slight tilt between the two pentamer rings, thus breaking the 2-fold rotational symmetry

TABLE III
*Crystallographic Statistics*

| Crystal/space group | SAP·**1**$_5$/P2$_1$ (Form A) | SAP$_2$·**1**$_5$/P1 (Form B) | SAP$_2$·**2**$_3$/P2$_1$ |
|---|---|---|---|
| Unit cell lengths (Å) | 94.7 × 70.0 × 101.1 | 96.7 × 105.3 × 146.0 | 77.9 × 95.1 × 164.3 |
| Unit cell angles (°) | 90, 97.1, 90.0 | 86.5, 78.2, 76.8 | 90.0, 98.7, 90.0 |
| Resolution (Å) | 60–2.00 | 100–2.20 | 100–3.00 |
| Total reflections[a] | 186,121 (17,285) | 534,468 (50,422) | 144,725 (11,626) |
| Unique reflections[a] | 84,221 (8,126) | 269,382 (26,464) | 45,367 (4,054) |
| Redundancy[a] | 2.2 (2.1) | 2.0 (1.9) | 3.2 (2.9) |
| Completeness (%)[a] | 94.5 (91.8) | 97.2 (95.6) | 95.1 (85.3) |
| $I/\sigma$[a] | 17.9 (6.3) | 15.5 (3.2) | 14.4 (2.2) |
| $R_{sym}$[a,b] | 0.047 (0.172) | 0.043 (0.231) | 0.071 (0.349) |
| $R_{work}$[c] | 0.219 (0.237) | 0.188 (0.229) | 0.228 (0.249) |
| $R_{free}$[d] | 0.251 (0.297) | 0.229 (0.287) | 0.282 (0.348) |
| Number of atoms | | | |
| Protein | 8,245 | 32,980 | 16,490 |
| Ligand | 64 | 300 | 95 |
| Solvent and ions | 483 | 487 | 20 |
| Root mean square deviations from ideal geometry | | | |
| Bond lengths (Å) | 0.006 | 0.007 | 0.007 |
| Bond angles (°) | 1.070 | 1.117 | 1.074 |
| Average temperature factors (Å$^2$) | | | |
| Wilson Plot | 18.1 | 35.1 | 75.2 |
| Protein[e] | 25.3 | 35.6 | 113.7 |
| Ligand[e] | 81.3 | 99.0 | 154.8 |
| Water[e] | 29.2 | 29.3 | |

[a] The values from the outermost resolution shell (SAP·**1**$_5$, 2.05–2.00; SAP$_2$·**1**$_5$, 2.28–2.20; SAP$_2$·**2**$_5$, 3.08–3.00) are given in parentheses.
[b] $R_{sym} = \Sigma_h\Sigma_i(|I_i(h) - \langle I(h)\rangle|)/\Sigma_h\Sigma_i I_i(h)$, where $I_i(h)$ is the $i^{th}$ integrated intensity of a given reflection and $\langle I(h)\rangle$ is the weighted mean of all measurements of $I(h)$.
[c] $R_{work} = \Sigma_h||F(h)_o| - |F(h)_c||/\Sigma_h|F(h)_o|$ for the 95% of the reflection data used in refinement.
[d] $R_{free} = \Sigma_h||F(h)_o| - |F(h)_c||/\Sigma_h|F(h)_o|$ for the 5% of he reflection data excluded from refinement.
[e] Temperature factors include TLS component as calculated by TLSANL (CCP4).

between opposing pentamers. The three central single bonds in compound **1** allow three additional degrees of torsional rotational freedom compared with the relatively rigid central piperazine ring found in compound **2**. The arrangement of protomers within each pentamer is the same in all complexes, and each pentamer forms a fairly rigid, planar unit. As a result, the binding interactions between each ligand and each $Ca^{2+}$-binding site, in combination with the geometric restrictions in the linker segment, control the relative orientation of each pentamer relative to the other.

In addition to the tilt angle between opposing pentameric rings, the relative rotational arrangement of each pentamer also varies in different complexes, when viewing the decameric complex along the 5-fold rotation axis (Fig. 5). In the complex with 2′-dAMP, the calcium ions from opposing pentamers are closely aligned. In comparison, the decameric complexes formed with compounds **1** and **2** show that the calcium ions from opposing pentamers are offset from each. The offset induces a rotation of 26° and 22° of one pentamer relative to other, when compared with the 2′-dAMP decameric complex. Although it would be of interest to perform a similar comparison with the decameric complex formed between SAP and the bivalent D-proline inhibitor (13), the coordinates for that structure have not been deposited in the Protein Data Bank.

It is important to note that there are no definite protein-protein interactions between opposing pentamers in either the SAP$_2$·**1**$_5$ or the SAP$_2$·**2**$_3$ complex. A possible exception to this may occur in the SAP$_2$·**2**$_3$ complex between the side chains of Lys$^{143}$ and His$^{78}$. It is possible to model conformations for both side chains that would allow them to form a hydrogen bond in the two opposing pairs of unliganded SAP protomers in the SAP$_2$·**2**$_3$ complex. Only two pairs of these hydrogen bonds can form between opposing pairs of unliganded protomers, because the separation between protomers is too large between opposing pairs of liganded SAP protomers. The presence of this hydrogen bond is somewhat speculative, because there is no definite electron density for the side chain of Lys$^{143}$ in the SAP$_2$·**2**$_3$ crystal structure to support the presence of this hydrogen bond. It should be noted that this interaction would be expected to be more stable at higher or more physiological pH values than that which is found in the crystal (pH 5.5). Lys$^{143}$ also forms the only direct protein-protein interaction bridging opposing SAP pentamers in the SAP$_2$·dAMP$_{10}$ complex, where the ϵ-amino group donates a hydrogen bond to a main chain carbonyl oxygen (16).

Apart from the potential hydrogen bond between Lys$^{143}$ and His$^{78}$, there may also be water-mediated interactions between opposing pentamers. The relatively low resolution and poor data quality of the SAP$_2$·**2**$_3$ complex does not allow for an analysis of water-mediated interactions. The higher resolution data for the SAP$_2$·**1**$_5$ complex helps to reveal well ordered solvent sites but likely fail to define partially ordered solvent sites. The model of solvent sites modeled from crystallographic data in the SAP$_2$·**1**$_5$ complex do not reveal a network of well ordered water molecules bridging opposing pentamers. The electron density for the solvent between pentamers suggests that the water molecules between opposing pentamers form a fairly dynamic ensemble.

Given the lack of evidence for rigid protein-protein or solvent-mediated interactions between opposing pentamers, it is likely that a wide range of rotational orientations between opposing pentamers are possible, depending on the structure and binding interactions of different cross-linking ligands. It is unclear at present whether different rotational orientations of opposing pentamers correlate with differences in biological activity. Because the formation of SAP decamers by bivalent molecules may be correlated with clearance from serum through cell surface receptors, it is interesting to consider whether different arrangements of pentamers may also be cleared at different rates. It may be that the tightest binding ligand will not be the one that promotes optimal clearance of SAP. Ongoing *in vivo* studies will help to address the therapeutic efficacy of compounds **1** and **2** in treating amyloid disorders such as Alzheimer disease.

Our crystal structure data pose several questions regarding the distribution of bound states in solution and in the crystal

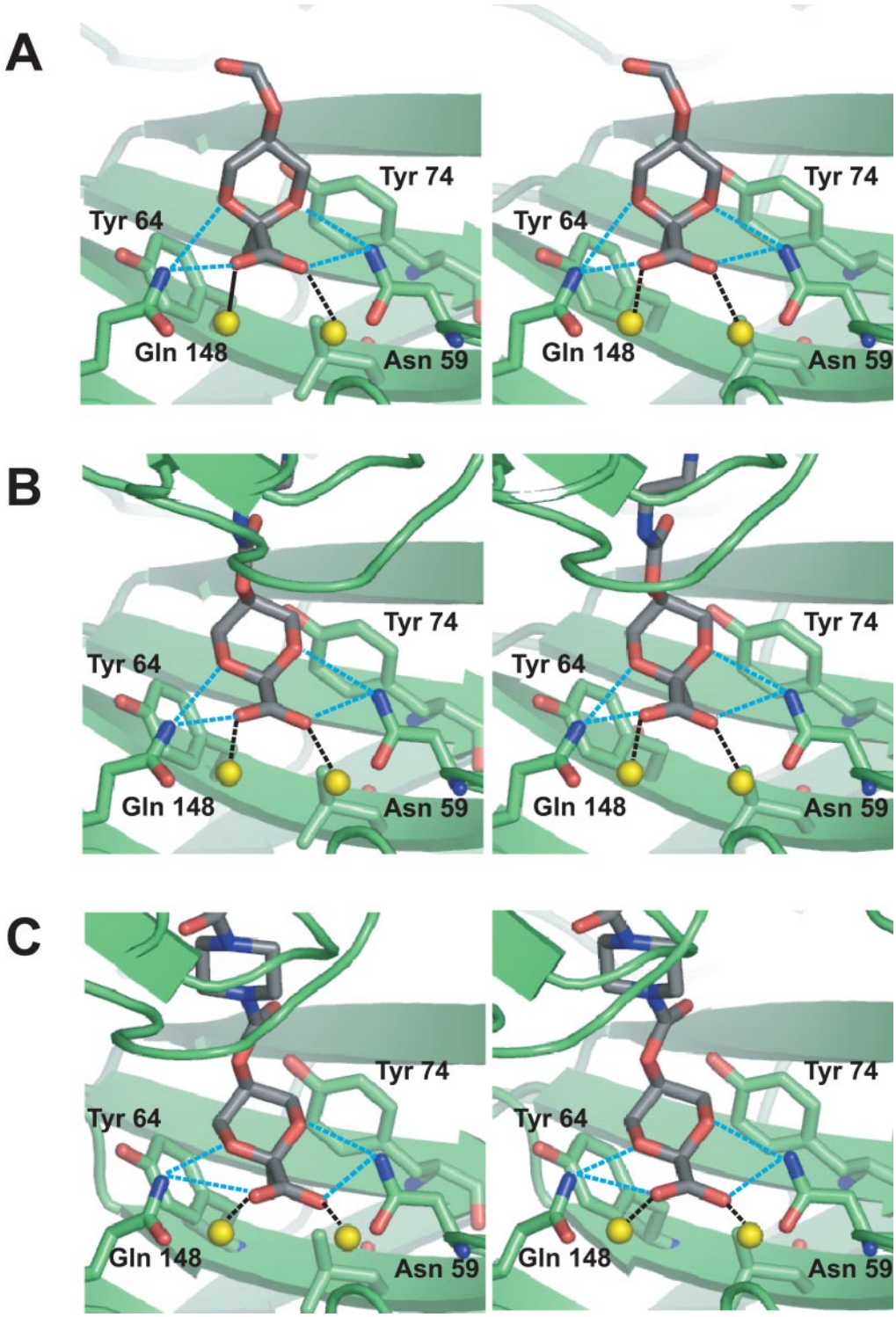


FIG. 3. **Stereoscopic views of the $Ca^{2+}$-binding site of SAP bound to compounds 1 (SAP·$1_5$ crystal form (*A*) and $SAP_2$·$1_5$ crystal form (*B*)) and 2 ($SAP_2$·$2_3$ (*C*)).** Carbon atoms in the ligands are colored *gray*, and in SAP are colored *green*. Oxygen and nitrogen atoms are colored *red* and *blue*, respectively. Calcium ions are represented by *yellow spheres*. Hydrogen bonds and calcium coordination bonds are denoted by *blue* and *black dashed lines* and *solid black lines*, respectively. Figs. 3–5 were prepared using PyMOL (32).

state that cannot be resolved at present. The most active compound **2** achieves its activity despite the presence of only three bivalent ligands in the face-to-face complex with SAP. If this crystal structure accurately represents the solution behavior of compound **2** with SAP, then the explanation for the higher activity of this compound is more complex than implied by the preceding discussion, and the thermodynamic model used to infer binding constants would need revision. Either positive or negative cooperativity effects might be in play, if the demands of accessible conformations of the ketal rings and tethers determine the different angular disposition of protein pentamers in the decameric complexes.

Alternatively, the tilted orientation of pentamer rings seen in the decameric complex with compound **2** may be the result of crystal packing forces as opposed to intrinsic conformational preferences in the tether of compound **2.** If true, compound **2** should form a decameric complex with the stoichiometry $SAP_2$·$\mathbf{2}_5$ in solution that is similar in structure to the decameric

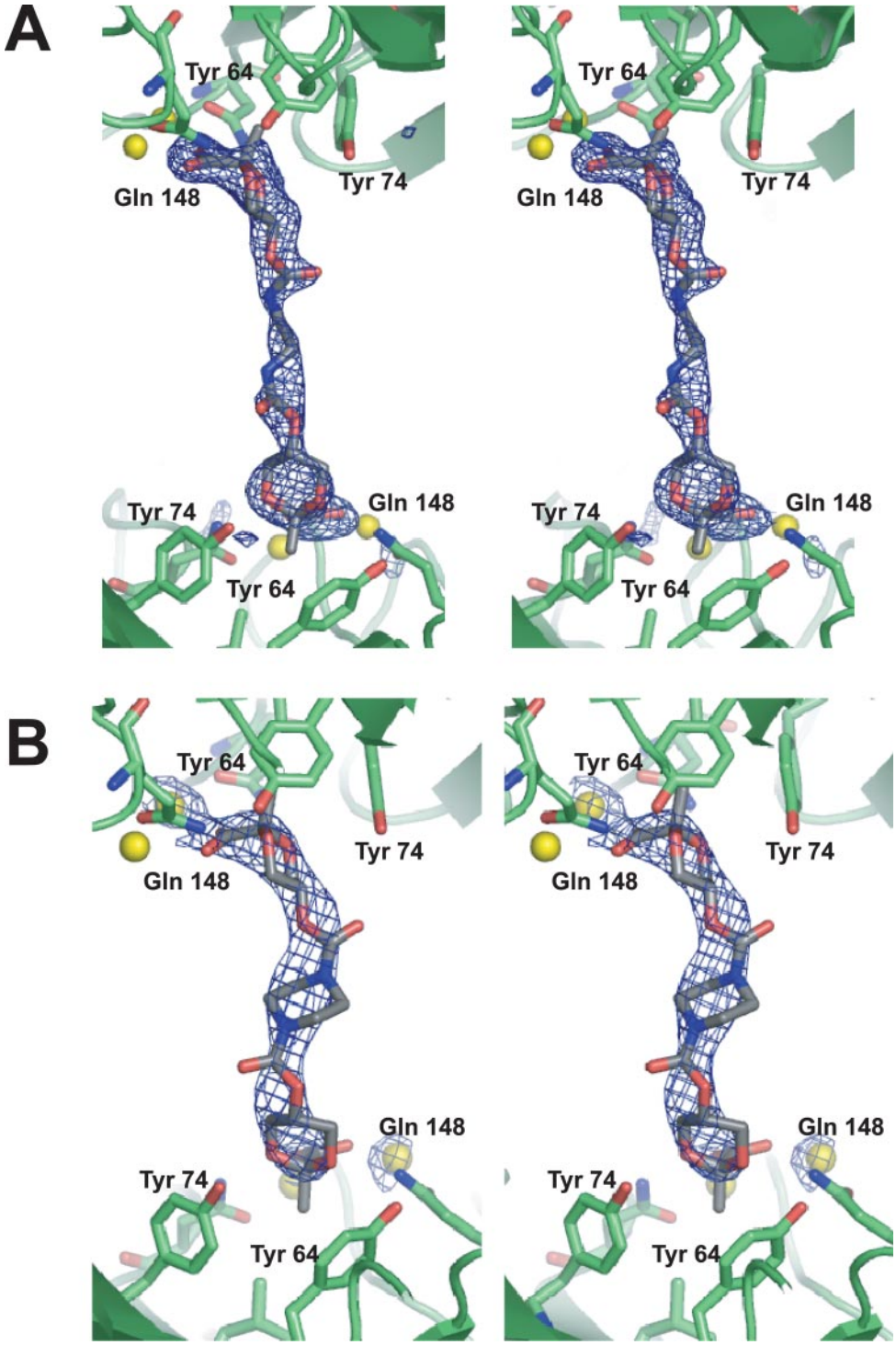


FIG. 4. **Stereoscopic views of electron density contoured around compounds 1 (*A*) ($SAP_2 \cdot \mathbf{1}_5$ crystal form B) and 2 (*B*) ($SAP_2 \cdot \mathbf{2}_3$) bridging two pentamers of SAP.** All of the atoms of the ligand were removed from the model before refinement and the calculation of a sigma-A weighted $|F_o| - |F_c|$ difference map (contoured at 3.0 and 2.5 $\sigma$ in *A* and *B*, respectively).

complex $SAP_2 \cdot \mathbf{1}_5$. This explanation is attractive because all of the binding sites would have uniform binding characteristics, thereby making it unnecessary to invoke negative or positive cooperativity between opposing pentamers as an explanation for the higher inhibitory activity of compound **2**.

A weakness of this interpretation is that there is no evidence indicating the presence of strong crystal packing forces capable of distorting a symmetrical decameric complex into the complex with pentamer rings tilted relative to each other and in which ligands are displaced from four binding sites. The solvent content of the three crystal forms are: $SAP \cdot \mathbf{1}_5$, 57%; $SAP_2 \cdot \mathbf{1}_5$, 59%; and $SAP_2 \cdot \mathbf{2}_3$, 52%, which are all within the normal range for protein crystals (29). Moreover, the pattern of crystal packing interactions in the $SAP_2 \cdot \mathbf{2}_3$ crystal form does not appear to strongly favor a tilted complex. It is of interest to note that in the crystal structure of SAP cross-linked by bivalent D-proline ligands (13), the tether length is not ideal, and a strained conformation appears to be adopted. In that case as well, there is no clear evidence indicating whether the strained conformation of the tether is induced by the geometric constraints on the system or whether crystal packing forces are involved.

To address these uncertainties about the solution composi-

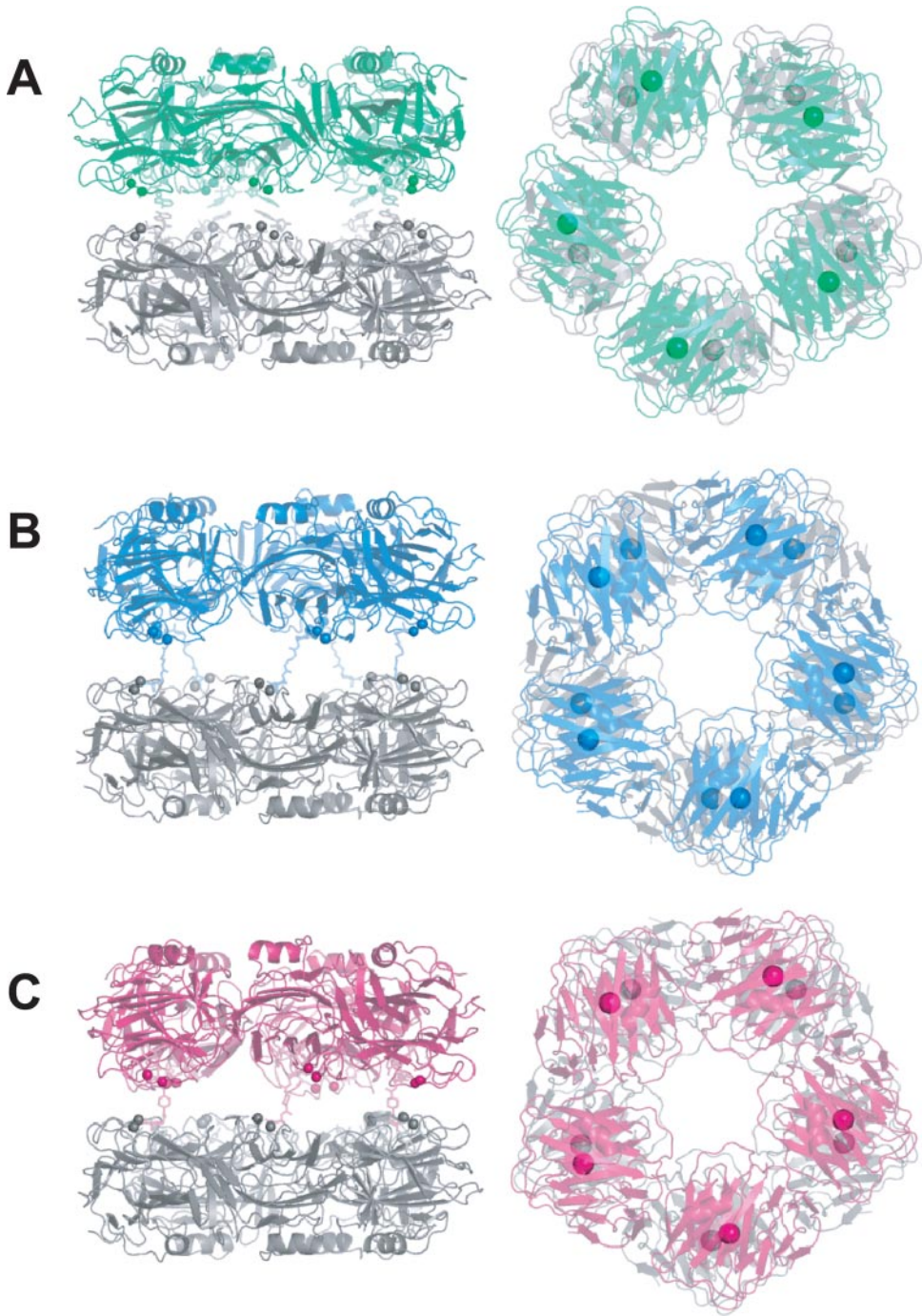


FIG. 5. **Decameric structures of SAP bound to 2′-dAMP (Protein Data Bank code 1LGN) (*A*), compound 1 ($SAP_2 \cdot \mathbf{1}_5$ crystal form B) (*B*), and compound 2 ($SAP_2 \cdot \mathbf{2}_3$) (*C*).** The orientation of the lower pentamer (colored *gray*) is the same for all molecules in the side and top views shown in the *left* and *right panels*, respectively. The center of mass for each protomer is drawn in the *right panel* as a *large sphere*.

tion of decameric complexes induced by compound **2** it would be helpful to determine the stoichiometry of ligand binding in complexes formed in solution using a technique that provides highly precise mass measurements. Nanoelectrospray ionization mass spectrometry studies have previously reported on the distribution of SAP oligomeric states in solution (30), but ligand binding studies pose a more difficult challenge. Fourier transform-ion cyclotron resonance mass spectrometry has been used to determine ligand binding stoichiometry in complexes with a total mass of ~40 kDa (31). However, the higher mass of the decameric complexes at ~250 kDa poses a severe challenge to the instrumentation currently available.

## CONCLUSIONS

Simple, achiral, bivalent ligands based on the pyruvate ketal of glycerol exhibit micromolar to submicromolar binding constants with SAP and induce the formation of face-to-face decameric complexes $SAP_2 \cdot \mathbf{1}_5$ and $SAP_2 \cdot \mathbf{2}_3$. Solution studies primarily using DLS, x-ray crystal structures, and a thermodynamic model establish that although ligand-protein interactions determine the nature of the cross-linking interactions, the orientation of protein protomers is determined by tether characteristics and that the requirements of the complex can affect the conformation of the pyruvate ketal ring. This work establishes a number of fundamental principles for the design

of novel cross-linking compounds that can exploit the thermodynamic advantages of multivalent binding while at the same time inducing the formation of specific aggregates with the geometric properties necessary for desirable therapeutic purposes.

*Acknowledgment*—We thank Isabelle Barrette-Ng for helpful discussions regarding this manuscript.

REFERENCES

1. Boas, U., and Heegaard, P. M. (2004) *Chem. Soc. Rev.* **33,** 43–63
2. Kitov, P. I., Sadowska, J. M., Mulvey, G., Armstrong, G. D., Ling, H., Pannu, N. S., Read, R. J., and Bundle, D. R. (2000) *Nature* **403,** 669–672
3. Fan, E. K., Zhang, Z. S., Minke, W. E., Hou, Z., Verlinde, C. L. M. J., and Hol, W. G. J. (2000) *J. Am. Chem. Soc.* **122,** 2663–2664
4. Zhang, Z., Merritt, E. A., Ahn, M., Roach, C., Hou, Z., Verlinde, C. L., Hol, W. G., and Fan, E. (2002) *J. Am. Chem. Soc.* **124,** 12991–12998
5. Pollock, R., and Clackson, T. (2002) *Curr. Opin. Biotechnol.* **13,** 459–467
6. Kitov, P. I., and Bundle, D. R. (2003) *J. Am. Chem. Soc.* **125,** 16271–16284
7. Gargano, J. M., Ngo, T., Kim, J. Y., Acheson, D. W., and Lees, W. J. (2001) *J. Am. Chem. Soc.* **123,** 12909–12910
8. Noursadeghi, M., Bickerstaff, M. C., Gallimore, J. R., Herbert, J., Cohen, J., and Pepys, M. B. (2000) *Proc. Natl. Acad. Sci. U. S. A.* **97,** 14584–14589
9. Bickerstaff, M. C., Botto, M., Hutchinson, W. L., Herbert, J., Tennent, G. A., Bybee, A., Mitchell, D. A., Cook, H. T., Butler, P. J., Walport, M. J., and Pepys, M. B. (1999) *Nat. Med.* **5,** 694–697
10. Gillmore, J. D., Hutchinson, W. L., Herbert, J., Bybee, A., Mitchell, D. A., Hasserjian, R. P., Yamamura, K., Suzuki, M., Sabin, C. A., and Pepys, M. B. (2004) *Immunology* **112,** 255–264
11. Tennent, G. A., Lovat, L. B., and Pepys, M. B. (1995) *Proc. Natl. Acad. Sci. U. S. A.* **92,** 4299–4303
12. Botto, M., Hawkins, P. N., Bickerstaff, M. C., Herbert, J., Bygrave, A. E., McBride, A., Hutchinson, W. L., Tennent, G. A., Walport, M. J., and Pepys, M. B. (1997) *Nat. Med.* **3,** 855–859
13. Pepys, M. B., Herbert, J., Hutchinson, W. L., Tennent, G. A., Lachmann, H. J., Gallimore, J. R., Lovat, L. B., Bartfai, T., Alanine, A., Hertel, C., Hoffmann, T., Jakob-Roetne, R., Norcross, R. D., Kemp, J. A., Yamamura, K., Suzuki, M., Taylor, G. W., Murray, S., Thompson, D., Purvis, A., Kolstoe, S., Wood, S. P., and Hawkins, P. N. (2002) *Nature* **417,** 254–259
14. Otwinowski, Z., and Minor, W. (1997) *Methods Enzymol.* **276,** 307–326
15. Collaborative Computational Project, N. (1994) *Acta Crystallogr. Sect. D Biol. Crystallogr.* **50,** 760–763
16. Hohenester, E., Hutchinson, W. L., Pepys, M. B., and Wood, S. P. (1997) *J. Mol. Biol.* **269,** 570–578
17. Vagin, A. A., and Teplyakov, A. (1997) *J. Appl. Crystallogr.* **30,** 1022–1025
18. Winn, M. D., Isupov, M. N., and Murshudov, G. N. (2001) *Acta Crystallogr. Sect. D Biol. Crystallogr.* **57,** 122–133
19. Navaza, J. (1994) *Acta Crystallogr. Sect. A* **50,** 157–163
20. Brunger, A. T., Adams, P. D., Clore, G. M., DeLano, W. L., Gros, P., Grosse-Kunstleve, R. W., Jiang, J. S., Kuszewski, J., Nilges, M., Pannu, N. S., Read, R. J., Rice, L. M., Simonson, T., and Warren, G. L. (1998) *Acta Crystallogr. Sect. D Biol. Crystallogr.* **54,** 905–921
21. McRee, D. E. (1999) *J. Struct. Biol.* **125,** 156–165
22. Morris, A. L., MacArthur, M. W., Hutchinson, E. G., and Thornton, J. M. (1992) *Proteins* **12,** 345–364
23. Hooft, R. W., Vriend, G., Sander, C., and Abola, E. E. (1996) *Nature* **381,** 272
24. Pepys, M. B., Booth, D. R., Hutchinson, W. L., Gallimore, J. R., Collins, P. M., and Hohenester, E. (1997) *Amyloid J. Protein Folding Disorders* **4,** 274–295
25. Thompson, D., Pepys, M. B., Tickle, I., and Wood, S. (2002) *J. Mol. Biol.* **320,** 1081–1086
26. Hutchinson, W. L., Hohenester, E., and Pepys, M. B. (2000) *Mol. Med.* **6,** 482–493
27. Emsley, J., White, H. E., O'Hara, B. P., Oliva, G., Srinivasan, N., Tickle, I. J., Blundell, T. L., Pepys, M. B., and Wood, S. P. (1994) *Nature* **367,** 338–345
28. Ashton, A. W., Boehm, M. K., Gallimore, J. R., Pepys, M. B., and Perkins, S. J. (1997) *J. Mol. Biol.* **272,** 408–422
29. Matthews, B. W. (1968) *J. Mol. Biol.* **33,** 491–497
30. Aquilina, J. A., and Robinson, C. V. (2003) *Biochem. J.* **375,** 323–328
31. Kitova, E. N., Kitov, P. I., Bundle, D. R., and Klassen, J. S. (2001) *Glycobiology* **11,** 605–611